# Quasiparticle interference patterns in bilayer graphene with trigonal warping

Vardan Kaladzhyan , 1,\* Frédéric Joucken, 2 Zhehao Ge, 2 Eberth A. Quezada-Lopez, 2
Takashi Taniguchi, 3 Kenji Watanabe , 4 Jairo Velasco, Jr., 2 and Cristina Bena 5

1 Department of Physics, University of Basel, Klingelbergstrasse 82, CH-4056 Basel, Switzerland

2 Department of Physics, University of California, Santa Cruz, California 95064, USA

3 International Center for Materials Nanoarchitectonics, National Institute for Materials Science, 1-1 Namiki, Tsukuba 305-0044, Japan

4 Research Center for Functional Materials, National Institute for Materials Science, 1-1 Namiki, Tsukuba 305-0044, Japan

5 Institut de Physique Théorique, Université Paris Saclay, CEA CNRS, Orme des Merisiers, 91190 Gif-sur-Yvette Cedex, France



(Received 19 May 2021; revised 10 December 2021; accepted 10 December 2021; published 20 December 2021)

We calculate the form of quasiparticle interference patterns in bilayer graphene within a low-energy description, taking into account perturbatively the trigonal warping terms. We introduce four different types of impurities localized on the A and B sublattices of the first and the second layer, and we obtain closed-form analytical expressions both in real and Fourier spaces for the oscillatory corrections to the local density of states generated by the impurities. Finally, we compare our findings with recent experimental and semianalytical *T*-matrix results from Joucken *et al.* [Nano Lett. **21**, 7100 (2021)], and we show that there is a very good agreement between our findings and the previous results, as well as with the experimental data.

DOI: 10.1103/PhysRevB.104.235425

## I. INTRODUCTION

In realistic materials, impurities and defects are ubiquitous players that often hinder the interpretation of experimental results when the impurity-associated broadening is larger than the level spacing. However, certain manifestations of their presence can be useful to reveal some interesting properties and to access the parameters of the underlying systems. For instance, Friedel oscillations in the local density of states (LDOS) [1], often referred to as "quasiparticle interference patterns," allow one to extract the Fermi momentum of the electrons, as well as to infer the dimension of the system under consideration. These oscillations arise as a result of impurity scattering processes and represent interferences between incoming and outgoing wave packets.

Quasiparticle interference patterns have been extensively studied, both theoretically and experimentally, in graphene, be it single layer or multilayer [2–17]. For instance, it was shown that in a single-layer graphene sheet, due to the chirality of the Dirac electrons, the correction to the local density of states in the presence of impurities decays as  $1/r^2$  [2,3,6,7], different from the 1/r behavior prevalent in other more standard two-dimensional systems [5,6]. However, as was demonstrated in Ref. [6], the 1/r decay is restored in bilayer graphene. Experimentally, quasiparticle interference patterns are accessible via Fourier-transform (FT) scanning tunneling microscopy [18,19].

It was anticipated theoretically [20–22] and confirmed experimentally [23–28] that there is a threefold symmetric warping of the bands in bilayer graphene, the so-called "trigonal warping." Originating from the interlayer coupling

between nondimer orbitals A1 and B2, the latter splits the Dirac points inherent in graphenelike systems into four Dirac points, as is shown in Fig. 1 for one of the valleys. Furthermore, as was demonstrated in Refs. [20,22,25–30], the trigonal warping can have important consequences for the physical properties of graphitic systems. It is worth noting that the effect of the trigonal warping observable in experiments is stronger as one approaches the Dirac points. Finally, note that some confusion regarding the orientation of the trigonal warping has been solved both theoretically [31] and experimentally [24].

In this paper we calculate analytically the quasiparticle interference patterns in bilayer graphene taking into account the trigonal warping terms. Using a first-order perturbative expansion in trigonal warping, and the T-matrix formalism [32–37], we find closed analytical expressions for the correction to the local density of states introduced by four distinct types of impurities localized at different sublattices and layers of the bilayer graphene. Our most interesting observations are that at the energies close to the Dirac points the real-space oscillations reflect the symmetry of the trigonal warping, and most saliently, one can extract in a closed analytical form the values of momenta at which the oscillations occur. By analyzing our findings both in the real and Fourier space, we provide a comparison with recent experiments and semianalytical calculations [24,38], and we show that our results are in good agreement with the experimental observations.

We proceed as follows: in Sec. II we derive the low-energy description of bilayer graphene, and in Sec. III we calculate perturbatively the bare retarded Green's function of the system in the real and Fourier space. In Sec. IV we apply the *T*-matrix formalism to compute the quasiparticle interference patterns and compare these findings with the experimental results, leaving the conclusions to Sec. V.

<sup>\*</sup>vardan.kaladzhyan@phystech.edu

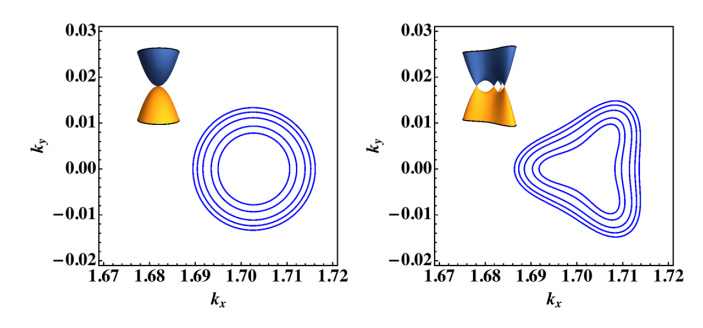


FIG. 1. Equal-energy contours for bilayer graphene in the absence and in the presence of trigonal warping (left and right panels, respectively). The corresponding band structures are shown as insets. In the presence of the trigonal warping the original Dirac point is split in four, but in our analysis we will consider energies above the point at which the four Dirac points merge.

#### II. LOW-ENERGY DESCRIPTION

We start by writing down the simplest lattice model for bilayer graphene [22,24]. In the basis  $\{\psi_k^{A1},\,\psi_k^{B1},\,\psi_k^{A2},\,\psi_k^{B2}\}$ , where A,B and 1,2 refer to sublattices and layers, respectively, we have

$$H(\mathbf{k}) \equiv \begin{pmatrix} 0 & -\gamma_0 f(\mathbf{k}) & 0 & -\gamma_3 f^*(\mathbf{k}) \\ -\gamma_0 f^*(\mathbf{k}) & 0 & \gamma_1 & 0 \\ 0 & \gamma_1 & 0 & -\gamma_0 f(\mathbf{k}) \\ -\gamma_3 f(\mathbf{k}) & 0 & -\gamma_0 f^*(\mathbf{k}) & 0 \end{pmatrix},$$
(1)

where we defined  $f(\mathbf{k}) \equiv e^{ik_y a/\sqrt{3}} + 2e^{-ik_y a/2\sqrt{3}}\cos\frac{k_x a}{2}$ , a=2.46 Å is the lattice constant, the intra- and interlayer hopping constants are denoted by  $\gamma_0=3.3$  and  $\gamma_1=0.42$  eV, respectively, and the trigonal warping parameter  $\gamma_3=-0.3$  eV. The sign of the latter stands for the warping orientation.

To derive a low-energy theory, we expand the Hamiltonian in Eq. (1) around  $K_s \equiv (s\frac{4\pi}{3a},0)$  points, where  $s=\pm$  is the valley index, and we get

$$f(\mathbf{k}) \approx -\frac{\sqrt{3}}{2} (sk_x - ik_y)a. \tag{2}$$

To simplify further the calculations, we divide the Hamiltonian above by  $\gamma_0 \sqrt{3}/2$ , thereby rendering it dimensionless, and we introduce  $q \equiv ka$ :

$$\mathcal{H}(q) = \begin{pmatrix} 0 & sqe^{-is\phi_q} & 0 & \gamma_{03}sqe^{+is\phi_q} \\ sqe^{+is\phi_q} & 0 & \gamma_{01} & 0 \\ 0 & \gamma_{01} & 0 & sqe^{-is\phi_q} \\ \gamma_{03}sqe^{-is\phi_q} & 0 & sqe^{+is\phi_q} & 0 \end{pmatrix},$$
(3)

where

$$\mathcal{H} \equiv \frac{2H}{\gamma_0\sqrt{3}}, \quad \gamma_{01} = \frac{2\gamma_1}{\gamma_0\sqrt{3}} \approx 0.15, \quad \gamma_{03} = \frac{\gamma_3}{\gamma_0} \approx -0.09.$$

For the sake of simplicity, above we introduced polar coordinates in momentum space, i.e., we replaced  $q = (q_x, q_y) \rightarrow$ 

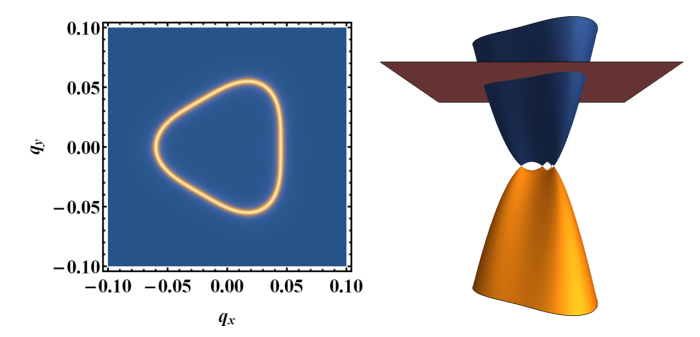


FIG. 2. The spectral function at  $\epsilon=0.018$  (equivalent to E=47 meV) and the band structure of bilayer graphene (left and right panels, correspondingly). The red plane on the right panel corresponds exactly to the energy at which we calculate the spectral function. We set  $\gamma_{01}\approx 0.15, \ \gamma_{03}\approx -0.09$ , which in dimensionful units corresponds to  $\gamma_1=0.42$  eV,  $\gamma_3=-3.3$  eV, and we take  $\delta=0.001$ .

$$(q,\,\phi_q),\,\,\,{
m where}\,\,\,q=\sqrt{q_x^2+q_y^2}\geqslant 0,\,\,{
m and}\,\,\,\phi_q\in[0,\,2\pi)\,\,\,{
m with}$$
  $e^{\pm is\phi_q}=rac{q_x\pm isq_y}{q}.$  The Hamiltonian in Eq. (3) provides a low-energy definition of the second of t

The Hamiltonian in Eq. (3) provides a low-energy description for bilayer graphene with trigonal warping. We find the unperturbed Green's function as  $\mathcal{G}_0(\boldsymbol{q},\epsilon) = [\epsilon - \mathcal{H}(\boldsymbol{q})]^{-1}$ , and we plot the spectral function  $-\frac{1}{\pi} \mathrm{Imtr} \mathcal{G}_0(\boldsymbol{q},\epsilon+i\delta)$  in Fig. 2. As expected, the latter reflects the trigonal warping of the bands.

# III. PERTURBATIVE CALCULATION OF THE RETARDED GREEN'S FUNCTION

In what follows we calculate the bare retarded Green's function in momentum space and in real space. The former is easily feasible; however, the latter requires a very complicated Fourier transform. Therefore, below, we adopt a different strategy, and we resort to a perturbative approach for both the momentum-space and real-space calculations.

## A. Momentum space

We rewrite the Hamiltonian in Eq. (3) as a sum of  $\mathcal{H}_0(q)$ , which is unperturbed by trigonal warping, and  $\mathcal{V}(q)$ , embodying the trigonal warping:

$$\mathcal{H}(\mathbf{q}) = \underbrace{\begin{pmatrix} 0 & sqe^{-is\phi_q} & 0 & 0\\ sqe^{+is\phi_q} & 0 & \gamma_{01} & 0\\ 0 & \gamma_{01} & 0 & sqe^{-is\phi_q}\\ 0 & 0 & sqe^{+is\phi_q} & 0 \end{pmatrix}}_{\mathcal{H}_0(\mathbf{q})} + \underbrace{\begin{pmatrix} 0 & 0 & 0 & \gamma_{03}sqe^{+is\phi_q}\\ 0 & 0 & 0 & 0\\ 0 & 0 & 0 & 0\\ \gamma_{03}sqe^{-is\phi_q} & 0 & 0 & 0 \end{pmatrix}}_{\mathcal{V}(\mathbf{q})}.$$
 (5)

Below we calculate the Matsubara Green's function  $G(i\omega, \mathbf{q}) \equiv [i\omega - \mathcal{H}(\mathbf{q})]^{-1}$  and then perform an analytic

continuation replacing  $i\omega \rightarrow \epsilon + i0^+$  to recover the retarded Green's function  $\mathcal{G}(\epsilon, \mathbf{q})$ .

In what follows we will consider that the trigonal warping term is small with respect to the bandwidth. This is indeed the case for the values considered here since  $\gamma_{03} = \gamma_3/\gamma_0 =$  $-0.09 \ll 1$ . Thus we can perform a perturbative expansions of our results in  $\gamma_{03}$ , and the first-order perturbation theory in  $\gamma_{03}$  yields

$$G(i\omega_n, \mathbf{q}) = [i\omega - \mathcal{H}_0(\mathbf{q}) - \mathcal{V}(\mathbf{q})]^{-1}$$
$$= \left[G_0^{-1}(i\omega, \mathbf{q}) - \mathcal{V}(\mathbf{q})\right]^{-1} \approx G_0(i\omega, \mathbf{q}) + G_1(i\omega, \mathbf{q}),$$

where  $G_1(i\omega, \mathbf{q}) \equiv G_0(i\omega, \mathbf{q}) \mathcal{V}(\mathbf{q}) G_0(i\omega, \mathbf{q})$  is the first-order correction in  $\gamma_{03}$ . Finally, in momentum space we have

$$G_0(i\omega, \boldsymbol{q}) = \frac{1}{D_q} \begin{pmatrix} g_0^{11} & (g_0^{21})^{\star} & (g_0^{31})^{\star} & (g_0^{41})^{\star} \\ g_0^{21} & g_0^{22} & g_0^{32} & (g_0^{31})^{\star} \\ g_0^{31} & g_0^{32} & g_0^{22} & (g_0^{21})^{\star} \\ g_0^{41} & g_0^{31} & g_0^{31} & g_0^{11} \end{pmatrix}.$$
(6)

Here,  $D_q \equiv (q^2 - (i\omega)^2 + i\omega\gamma_{01})(q^2 - (i\omega)^2 - i\omega\gamma_{01})$ , while  $g_0^{ij}$  denotes the (ij)th element of the matrix  $g_0$ , with

$$g_0^{11} \equiv i\omega ((i\omega)^2 - \gamma_{01}^2) - i\omega q^2, \quad g_0^{22} \equiv (i\omega)^3 - (i\omega)q^2,$$

$$g_0^{21} \equiv (i\omega)^2 \cdot sqe^{is\phi_q} - sq^3e^{is\phi_q}, \quad g_0^{31} \equiv i\omega\gamma_{01} \cdot sqe^{is\phi_q},$$

$$g_0^{32} \equiv (i\omega)^2\gamma_{01}, \quad g_0^{41} \equiv \gamma_{01} \cdot q^2e^{2is\phi_q}.$$
(7)

We use the  $\star$  symbol to denote replacing  $\phi_q \to -\phi_q$ , e.g.,  $(g_0^{31})^* = i\omega\gamma_{01} \cdot sqe^{-is\phi_q}$ . The first-order correction in trigonal warping is given by

$$G_{1}(i\omega, \boldsymbol{q}) = \frac{\gamma_{03}}{D_{q}^{2}} \begin{pmatrix} g_{1}^{11} & (g_{1}^{21})^{\star} & (g_{1}^{31})^{\star} & (g_{1}^{41})^{\star} \\ g_{1}^{21} & g_{1}^{22} & (g_{1}^{32})^{\star} & (g_{1}^{31})^{\star} \\ g_{1}^{31} & g_{1}^{32} & g_{1}^{22} & (g_{1}^{21})^{\star} \\ g_{1}^{41} & g_{1}^{31} & g_{1}^{21} & g_{1}^{21} \end{pmatrix}, (8)$$

where  $g_1^{ij}$  are defined in Appendix A2.

## B. Bare retarded Green's function in real space

In this section we calculate the Fourier transform of the Matsubara Green's function obtained perturbatively in the previous section. For this we need to calculate the two following integrals:

$$G(i\omega, \mathbf{r}) = \underbrace{\int_{0}^{+\infty} \frac{q dq}{2\pi} \int_{0}^{2\pi} \frac{d\phi_{q}}{2\pi} G_{0}(i\omega, \mathbf{q}) e^{iqr\cos(\phi_{q} - \phi_{r})}}_{G_{0}(i\omega, \mathbf{r})} + \underbrace{\int_{0}^{+\infty} \frac{q dq}{2\pi} \int_{0}^{2\pi} \frac{d\phi_{q}}{2\pi} G_{1}(i\omega, \mathbf{q}) e^{iqr\cos(\phi_{q} - \phi_{r})}}_{G_{1}(i\omega, \mathbf{r})}.$$

Above we introduced polar coordinates in real space, as well as in momentum space, i.e.,  $\mathbf{r} = (x, y) \rightarrow (r, \phi_r)$ , where  $r \ge$ 0 and  $\phi_r \in [0, 2\pi)$ . For the sake of brevity, we leave the final real-space form of the Green's functions, as well as the lengthy integral calculations to Appendixes B1 and B2.

## IV. QUASIPARTICLE INTERFERENCE PATTERNS

In what follows we introduce localized delta-function impurities into the system, and we calculate the associated quasiparticle interference patterns via the T-matrix formalism. To simplify the derivation, we assume that impurities are localized on a specific sublattice and in a specific layer, and we define their amplitudes as

where U denotes the magnitude of the impurity potential. We should note that we consider the effect of a single impurity alone, or equivalently a very low impurity concentration. To first approximation, the impurity concentration will affect the results by broadening the energy, i.e.,  $i\omega \rightarrow E + i\delta$ , where  $\delta$  embodies the broadening. In our analytics we set  $\delta = 0$ , thereby assuming that there is no additional disorder in the system except for the single localized impurity inducing the ripples in the local density of states. To obtain reasonable results, the disorder broadening  $\delta$  should be much smaller than the energy E at which we observe the local density of states. In other words, as long as the disorder concentration is small enough to avoid interference between the ripples in the local density of states originating from different impurities, the results are valid.

Below we proceed in two steps: First, with the help of the real-space form of the Green's function defined in Eqs. (9), (B1), and (B7)–(B14), we compute the T matrix that accounts for all-order impurity scattering processes. Second, we find the correction to the local density of states in the presence of impurities.

## A. T matrix

To find the T matrix, we need to evaluate the following expression [32–37]:

$$T(i\omega) = \left[\mathbb{I} - V \cdot \lim_{r \to 0} G(i\omega, r)\right]^{-1} V,\tag{11}$$

where  $G(i\omega, \mathbf{r}) \equiv G_0(i\omega, \mathbf{r}) + G_1(i\omega, \mathbf{r})$ , and  $V = V_{A1}$ ,  $V_{B1}$ ,  $V_{A2}$ ,  $V_{B2}$ , depending on the chosen impurity type. The firstorder correction to the Green's function does not contribute to the T matrix, since  $\lim_{r\to 0} G_1(i\omega, r) = 0$  due to the angular parts. Thus the corresponding T matrices are given by

where we defined

$$f(i\omega) \equiv \frac{U}{1 - U \lim_{r \to 0} \left[ i\omega \left( (i\omega)^2 - \gamma_{01}^2 \right) I_{00} - i\omega I_{03} \right]}, \quad (13)$$

$$g(i\omega) \equiv \frac{U}{1 - U \lim_{r \to 0} \left[ (i\omega)^3 I_{00} - i\omega I_{03} \right]}.$$
 (14)

We leave the calculation of the limits in Eqs. (13) and (14) to Appendix C, and we present the final result here:

$$\lim_{r \to 0} I_{00} = \frac{1}{4\pi \gamma_{01} i\omega} (\Omega_{+} - \Omega_{-}), \tag{15}$$

$$\lim_{r \to \mathbf{0}} I_{03} = -\frac{1}{4\pi \gamma_{01} i\omega} \sum_{\sigma = +} \sigma \left[ \gamma_{\varepsilon} \Omega_{\sigma}^2 + \Omega_{\sigma}^2 \ln \frac{\Omega_{\sigma} a}{2} \right], \quad (16)$$

where  $\gamma_{\mathcal{E}}$  is the Euler-Mascheroni constant,  $\Omega_{\sigma} \equiv \sqrt{i\omega(\pm\gamma_{01}-i\omega)}$ , and the lattice constant a is used as an infrared cutoff. Substituting Eqs. (15) and (16) into Eqs. (13) and (14), we obtain the final analytical form for  $f(i\omega)$  and  $g(i\omega)$ .

## B. Local density of states

To find the first-order correction in  $\gamma_{03}$  to the local density of states, we use Eq. (9), and we proceed as follows:

$$\delta\rho(i\omega, \mathbf{r}) = -\frac{1}{\pi} \operatorname{Imtr}_{1}[G(i\omega, \mathbf{r})T(i\omega)G(i\omega, -\mathbf{r})]$$

$$\approx -\frac{1}{\pi} \operatorname{Imtr}_{1}[G_{0}(i\omega, \mathbf{r})T(i\omega)G_{0}(i\omega, -\mathbf{r})$$

$$+ G_{0}(i\omega, \mathbf{r})T(i\omega)G_{1}(i\omega, -\mathbf{r})$$

$$+ G_{1}(i\omega, \mathbf{r})T(i\omega)G_{0}(i\omega, -\mathbf{r})], \qquad (17)$$

where we only take the trace of the *first-layer* components of the matrix, i.e.,  $\operatorname{tr}_1 M = M_{11} + M_{22}$ . We choose to calculate only a partial trace because the scanning tunneling microscope tip measures mostly the electronic density of states of the topmost layer. Since we are dealing with a perturbative calculation in  $\gamma_{03}$  up to the first order, we omitted the term  $G_1(i\omega, \mathbf{r})T(i\omega)G_1(i\omega, -\mathbf{r})$  proportional to  $\gamma_{03}^2$ . Note also that  $G_0(i\omega, \mathbf{r})$  and  $G_1(i\omega, \mathbf{r})$  were calculated in polar coordinates and thus replacing  $\mathbf{r} \to -\mathbf{r}$  is equivalent to  $\phi_r \to \pi + \phi_r$ . We also keep in mind that to calculate the physical response, we should use the retarded Green's functions, in other words, we should replace  $i\omega \to \epsilon + i\delta$ , where  $\epsilon$  is the energy and  $\delta \to +0$  is a positive infinitesimal shift.

## 1. Real space

Considering the form of the T matrix presented in Eq. (12), we can calculate analytically via Eq. (17) the corrections to the local density of states induced by each type of impurity. The exact analytical expressions for  $\delta\rho_{A1}(\epsilon,r,\phi_r)$ ,  $\delta\rho_{B1}(\epsilon,r,\phi_r)$ , and  $\delta\rho_{B2}(\epsilon,r,\phi_r)$  can be found using Eq. (17) and Appendixes B and C. We plot the corresponding expressions in Fig. 3. We should note that the value of U chosen

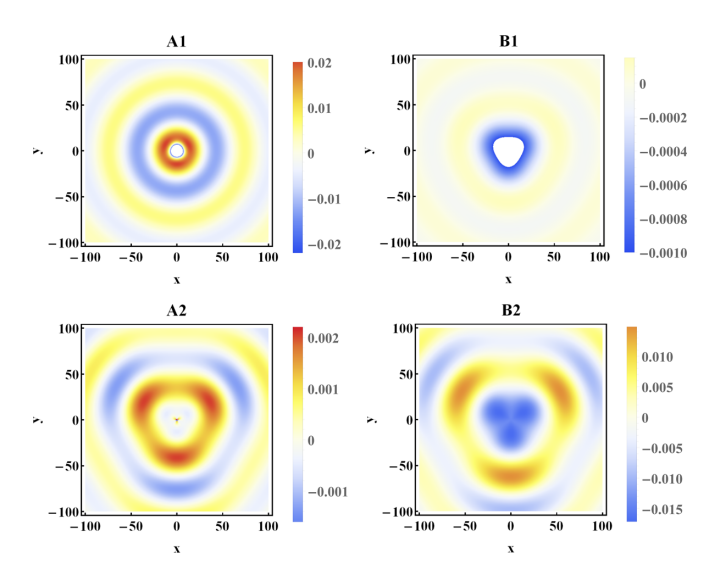


FIG. 3. Corrections to the local density of states calculated for A1, B1, A2, and B2 impurities, plotted as a function of x and y taken in the units of interatomic distance  $a^* = a/\sqrt{3} = 1.42$  Å. We set  $\gamma_{01} \approx 0.15$ ,  $\gamma_{03} \approx -0.09$ ,  $U \approx -105$ ,  $\epsilon \approx 0.018$ , which in dimensionful units corresponds to  $\gamma_1 = 0.42$  eV,  $\gamma_3 = -3.3$  eV, U = -300 eV, E = 50 meV.

to obtain these results is renormalized by the cutoff that is used for the low-energy theory. In this respect, the value of U should not be perceived as the literal amplitude of the defect potential. In Appendix E we discuss the dependence of the real-space oscillations on the value of U. To sum up the point of this, the value of U affects the amplitudes of the oscillations but does not alter their periodicity in the asymptotic limit.

We can clearly see that the panels for A2 and B2 impurities in Fig. 3 show strong threefold-symmetric features originating from the trigonal warping terms. Using the asymptotic forms of the local density of states calculated at  $r \to +\infty$  from Eqs. (D1)–(D4) shown in Appendix D, we present below their simplified forms at energies such that  $0 < \epsilon \ll \gamma_{01}$ . In this range of energies we can neglect the exponentially fast decaying terms, i.e., the terms containing  $e^{-2\Omega_+ r}$  factors, and thus we get

$$\delta \rho_{A1} = \frac{1}{\pi} \text{Im} \left[ \frac{f(\epsilon)}{32\pi \epsilon} \Omega_{-} \frac{\gamma_{01} + \gamma_{03} \Omega_{-} \sin 3\phi_r}{r} e^{-2\Omega_{-}r} \right], \quad (18)$$

$$\delta \rho_{B1} = \frac{1}{\pi} \text{Im} \left[ \frac{g(\epsilon)}{32\pi} \gamma_{01} \frac{\epsilon + \gamma_{03} \Omega_{-} \sin 3\phi_{r}}{\Omega_{-} r} e^{-2\Omega_{-} r} \right], \tag{19}$$

$$\delta \rho_{A2} = \frac{1}{\pi} \text{Im} \left[ \frac{g(\epsilon)}{32\pi} \gamma_{01} \frac{\epsilon - \gamma_{03} \Omega_{-} \sin 3\phi_r}{\Omega_{-} r} e^{-2\Omega_{-} r} \right], \tag{20}$$

$$\delta \rho_{B2} = -\frac{1}{\pi} \text{Im} \left[ \frac{f(\epsilon)}{32\pi} \gamma_{01} \frac{\gamma_{01} - \gamma_{03} \Omega_{-} \sin 3\phi_{r}}{\Omega_{-} r} e^{-2\Omega_{-} r} \right]. \tag{21}$$

Note that for negative energies  $\epsilon < 0$  we should keep the terms with  $e^{-2\Omega_+ r}$  factors and discard those with  $e^{-2\Omega_- r}$ . Furthermore, it is worth emphasizing that the asymptotic expansions above describe the LDOS well only at large distances from the origin, namely, at  $r \gg \max(\frac{1}{2|\Omega_+|}, \frac{1}{2|\Omega_-|})$ . Therefore, to recover correctly the features in the vicinity of the impurity, we have to consider the full expressions provided in Eqs. (D1)–(D4).

The results presented in Fig. 3 are in nearly perfect agreement with the semianalytical T-matrix calculations based on a lattice model and presented in Refs. [38,39].

Furthermore, the orientation of the triangles flips with the sign of  $\gamma_{03}$ . This can be straightforwardly seen in the asymptotic forms of the corrections derived in Eqs. (18)–(21) for  $r \to +\infty$ , which can be rewritten in the simplified form

$$\delta \rho \sim \frac{\alpha + \beta \gamma_{03} \sin 3\phi_r}{r} e^{-\Omega r},$$
 (22)

where  $\alpha$ ,  $\beta$ , and  $\Omega$  can be inferred from Eqs. (18)–(21).

In the equation above, the term generated by trigonal warping is proportional to  $\sin 3\phi_r/r$ , while the first term proportional to 1/r is known in the literature as the quasiparticle

interference pattern for bilayer graphene in the absence of trigonal warping [6].

We should note that, as expected from the band structure, the smaller the energy at which we calculate the quasiparticle interference patterns, the more visible are the effects of the trigonal warping.

## 2. Momentum space

In what follows we analyze theoretically momentum-space quasiparticle interference patterns experimentally accessible via Fourier-transform scanning tunneling microscopy. It is clear that the Fourier transform of Eq. (22) yields both rotationally symmetric and angular-dependent parts. We Fourier-transform Eqs. (18)–(21), and we get

$$\delta\rho_{A1} = \frac{1}{2\pi i} \frac{f(\epsilon)\Omega_{-}[\gamma_{01}\mathcal{F}_{0}(p,2\Omega_{-}) + \gamma_{03}\Omega_{-}\mathcal{F}_{1}(\boldsymbol{p},2\Omega_{-})] - f^{*}(\epsilon)\Omega_{-}^{*}[\gamma_{01}\mathcal{F}_{0}(p,2\Omega_{-}^{*}) + \gamma_{03}\Omega_{-}^{*}\mathcal{F}_{1}(\boldsymbol{p},2\Omega_{-}^{*})]}{32\pi\epsilon},$$
 (23)

$$\delta \rho_{B1} = \frac{1}{2\pi i} \gamma_{01} \frac{\frac{g(\epsilon)}{\Omega_{-}} [\epsilon \mathcal{F}_{0}(p, 2\Omega_{-}) + \gamma_{03}\Omega_{-}\mathcal{F}_{1}(\boldsymbol{p}, 2\Omega_{-})] - \frac{g^{*}(\epsilon)}{\Omega_{-}^{*}} [\epsilon \mathcal{F}_{0}(p, 2\Omega_{-}^{*}) + \gamma_{03}\Omega_{-}^{*}\mathcal{F}_{1}(\boldsymbol{p}, 2\Omega_{-}^{*})]}{32\pi}, \tag{24}$$

$$\delta \rho_{A2} = \frac{1}{2\pi i} \gamma_{01} \frac{\frac{g(\epsilon)}{\Omega_{-}} [\epsilon \mathcal{F}_{0}(p, 2\Omega_{-}) - \gamma_{03}\Omega_{-}\mathcal{F}_{1}(\boldsymbol{p}, 2\Omega_{-})] - \frac{g^{*}(\epsilon)}{\Omega_{-}^{*}} [\epsilon \mathcal{F}_{0}(p, 2\Omega_{-}^{*}) - \gamma_{03}\Omega_{-}^{*}\mathcal{F}_{1}(\boldsymbol{p}, 2\Omega_{-}^{*})]}{32\pi}, \tag{25}$$

$$\delta\rho_{B2} = -\frac{1}{2\pi i} \gamma_{01} \frac{\frac{f(\epsilon)}{\Omega_{-}} [\gamma_{01} \mathcal{F}_{0}(p, 2\Omega_{-}) - \gamma_{03} \Omega_{-} \mathcal{F}_{1}(\mathbf{p}, 2\Omega_{-})] - \frac{f^{*}(\epsilon)}{\Omega_{-}^{*}} [\gamma_{01} \mathcal{F}_{0}(p, 2\Omega_{-}^{*}) - \gamma_{03} \Omega_{-}^{*} \mathcal{F}_{1}(\mathbf{p}, 2\Omega_{-}^{*})]}{32\pi},$$
(26)

where  $\mathcal{F}_0$  and  $\mathcal{F}_1$  are calculated in Appendix D and are given by

$$\mathcal{F}_0(p,\Omega) = \frac{2\pi}{\Omega} \frac{1}{\sqrt{1 + \frac{p^2}{\Omega^2}}},\tag{27}$$

 $\mathcal{F}_1(\mathbf{p},\Omega) = 2\pi i \sin 3\phi_n$ 

$$\times \frac{p^{2}\left(-3+\sqrt{1+\frac{p^{2}}{\Omega^{2}}}\right)+4\Omega^{2}\left(-1+\sqrt{1+\frac{p^{2}}{\Omega^{2}}}\right)}{p^{3}\sqrt{1+\frac{p^{2}}{\Omega^{2}}}}.$$
(28)

Using these definitions and the Fourier transforms in Eqs. (23)–(26), we infer the position of the ringlike resonance in momentum space

$$p_{\rm res} = -2i\Omega_{-} = 2\sqrt{\epsilon(\gamma_{01} + \epsilon)}. \tag{29}$$

Above, we denoted  $\epsilon \equiv \frac{2E}{\gamma_0\sqrt{3}}$ , where *E* is the energy at which we calculate the response. In the left panel of Fig. 4 we plot the absolute of the sum of Fourier transforms in Eqs. (23)–(26) simulating a large-sample experiment in which

all types of impurities contribute to the local response. In the right panel of Fig. 4 we show the corresponding experimental measurement in dimensionless momentum space  $(p_x, p_y) = (k_x a, k_y a)$ , where the lattice constant a = 2.46 Å. We see that the analytical and experimental results are in a good agreement, i.e.,  $p_{\text{res}}^{\text{exp}} \approx 0.095$  is very close to the analytically calculated value using Eq. (29):

$$p_{\text{res}} = 2\sqrt{\frac{2E}{\gamma_0\sqrt{3}} \left(\frac{2\gamma_1}{\gamma_0\sqrt{3}} + \frac{2E}{\gamma_0\sqrt{3}}\right)} \approx 0.1,$$
 (30)

where we set E = 47 meV.

To derive the FT LDOS, we used the asymptotic expansions in Eqs. (18)–(21), and since we work with asymptotic expansions at  $r \to +\infty$  obtained within a low-energy approximation, the hexagonal shape of the resonance is lost in the analytically computed FT versus the experimental one (left versus right panels of Fig. 4). In Eqs. (23)–(26) the reminiscence of hexagonal symmetries is carried solely by the phase factor  $\sin 3\phi_p$  in the definition of  $\mathcal{F}_1(p,\Omega)$ , and it is reflected in the inset of the left panel of Fig. 4.

The results obtained above are also qualitatively consistent with the numerical *T*-matrix calculations presented in Ref. [38], with the only difference being the hexagonal shape of the resonance in the latter. This discrepancy stems from the fact that in this paper we use a low-energy approximation, while

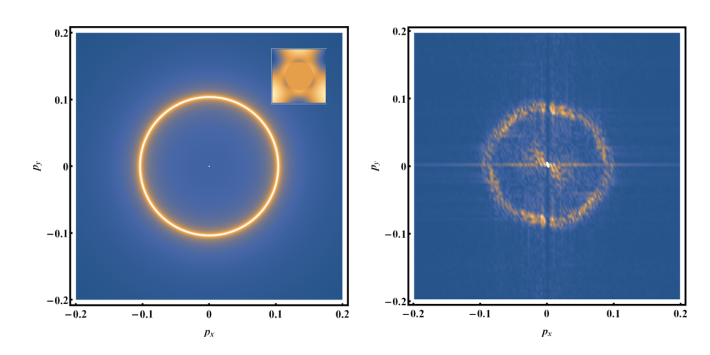


FIG. 4. Analytically calculated and experimentally measured quasiparticle interference patterns are presented in dimensionless momentum space in the left and right panels, respectively. The analytical panel and its inset are obtained respectively as the absolute value, and the imaginary part of the sum of the responses to different types of impurities given in Eqs. (23)-(26) (normalized by the response without trigonal warping). The inset (the imaginary part of the result) demonstrates the hexagonal symmetry of the problem. The right panel shows a fast Fourier transform of an experimental scanning tunneling microscopy dI/dV map obtained on Bernal-stacked bilayer graphene, reproduced from Fig. 2g of Ref. [38] (see Ref. [38] for experimental details). It was acquired at E = 47 meV, within the valence band. Both panels show a ringlike resonance appearing at  $p_{\rm res} \approx 0.1$  given by Eq. (30) and defined by the energy at which the local density of states is calculated, as well as by the intra- and interlayer coupling constants. We take the same values of parameters as in Fig. 2g in Ref. [38]:  $\gamma_0 = 3.3 \text{ eV}$ ,  $\gamma_1 = 0.42 \text{ eV}$ ,  $\gamma_3 = -0.3 \text{ eV}$ , E = 47 meV. Additionally, we set U = -300 eV, while in Ref. [38] U = -10 eV.

the numerical T-matrix calculations were performed within a lattice model.

#### V. CONCLUSIONS

We have calculated analytically the form of the quasiparticle interference patterns in bilayer graphene for four types of impurities localized on different layers and sublattices, taking into account perturbatively the trigonal warping of the bands. First and foremost, our results both in real space and in Fourier space are in good agreement with the experimental measurements and T-matrix-based semianalytical simulations of such patterns [24,38]. Most importantly, the fact that our analytical results can be expressed in closed form provides us with an understanding of the origin of the observed triangular features in real space. Thus we clearly see that they originate in the trigonal warping terms and flip orientation when the trigonal warping is changing sign. Also our results allow us to predict the value of the momentum corresponding to the ringlike resonances visible in momentum space and to the real-space oscillations; this seems to be independent of the value of the trigonal warping.

#### ACKNOWLEDGMENTS

J.V.J. acknowledges support from the National Science Foundation under Award No. DMR-1753367 and the Army Research Office under Contract No. W911NF-17-1-0473.

## APPENDIX A: GREEN'S FUNCTIONS IN MOMENTUM SPACE

## 1. Zeroth order

$$G_{0}(i\omega, \boldsymbol{q}) = \frac{1}{(q^{2} - (i\omega)^{2} + i\omega\gamma_{01})(q^{2} - (i\omega)^{2} - i\omega\gamma_{01})} \begin{pmatrix} g_{0}^{11} & (g_{0}^{21})^{\star} & (g_{0}^{31})^{\star} & (g_{0}^{41})^{\star} \\ g_{0}^{21} & g_{0}^{22} & g_{0}^{32} & (g_{0}^{31})^{\star} \\ g_{0}^{31} & g_{0}^{32} & g_{0}^{22} & (g_{0}^{21})^{\star} \\ g_{0}^{41} & g_{0}^{31} & g_{0}^{21} & g_{0}^{21} & g_{0}^{11} \end{pmatrix},$$
(A1)

with  $g_0^{ij}$  denoting the (ij)th element of the matrix  $g_0$ .

$$g_0^{11} \equiv i\omega \left( (i\omega)^2 - \gamma_{01}^2 \right) - i\omega q^2, \quad g_0^{22} \equiv (i\omega)^3 - (i\omega)q^2, \quad g_0^{21} \equiv (i\omega)^2 \cdot sqe^{is\phi_q} - sq^3e^{is\phi_q}, \quad g_0^{31} \equiv i\omega\gamma_{01} \cdot sqe^{is\phi_q},$$

$$g_0^{32} \equiv (i\omega)^2\gamma_{01}, \quad g_0^{41} \equiv \gamma_{01} \cdot q^2e^{2is\phi_q}.$$
(A2)

The symbol  $\star$  denotes replacing  $\phi_q \to -\phi_q$ , e.g.,  $(g_0^{31})^{\star} = i\omega\gamma_{01} \cdot sqe^{-is\phi_q}$ .

## 2. First order

The first-order correction in trigonal warping is given by

$$G_{1}(i\omega,\boldsymbol{q}) = \frac{\gamma_{03}}{(q^{2} - (i\omega)^{2} + i\omega\gamma_{01})^{2}(q^{2} - (i\omega)^{2} - i\omega\gamma_{01})^{2}} \begin{pmatrix} g_{1}^{11} & (g_{1}^{21})^{2} & (g_{1}^{31})^{2} & (g_{1}^{41})^{2} \\ g_{1}^{21} & g_{1}^{22} & (g_{1}^{32})^{*} & (g_{1}^{31})^{*} \\ g_{1}^{31} & g_{1}^{32} & g_{1}^{22} & (g_{1}^{21})^{*} \\ g_{1}^{41} & g_{1}^{31} & g_{1}^{21} & g_{1}^{21} \end{pmatrix},$$

where

$$g_1^{11} \equiv -\gamma_{01}i\omega[sq^5e^{3is\phi_q} + sq^5e^{-3is\phi_q}] - \gamma_{01}i\omega(\gamma_{01}^2 - (i\omega)^2)[sq^3e^{3is\phi_q} + sq^3e^{-3is\phi_q}], \tag{A3}$$

$$g_1^{22} \equiv -\gamma_{01}i\omega \left[ sq^5 e^{3is\phi_q} + sq^5 e^{-3is\phi_q} \right] + \gamma_{01}(i\omega)^3 \left[ sq^3 e^{3is\phi_q} + sq^3 e^{-3is\phi_q} \right], \tag{A4}$$

$$g_1^{21} \equiv -\gamma_{01} \left[ q^6 e^{4is\phi_q} \right] + \gamma_{01} (i\omega)^2 \left[ q^4 e^{4is\phi_q} - q^4 e^{-2is\phi_q} \right] - \gamma_{01} (i\omega)^2 \left( \gamma_{01}^2 - (i\omega)^2 \right) \left[ q^2 e^{-2is\phi_q} \right], \tag{A5}$$

$$g_1^{31} \equiv i\omega \left[q^6 e^{-2is\phi_q}\right] + \gamma_{01}^2 i\omega \left[q^4 e^{4is\phi_q}\right] + i\omega \left(\gamma_{01}^2 - 2(i\omega)^2\right) \left[q^4 e^{-2is\phi_q}\right] - (i\omega)^3 \left(\gamma_{01}^2 - (i\omega)^2\right) \left[q^2 e^{-2is\phi_q}\right], \tag{A6}$$

$$g_1^{32} \equiv \left[ sq^7 e^{-3is\phi_q} \right] - 2(i\omega)^2 \left[ sq^5 e^{-3is\phi_q} \right] + (i\omega)^4 \left[ sq^3 e^{-3is\phi_q} \right] + \gamma_{01}^2 (i\omega)^2 \left[ sq^3 e^{3is\phi_q} \right], \tag{A7}$$

$$g_1^{41} \equiv \gamma_{01}^2 \left[ sq^5 e^{5is\phi_q} \right] + (i\omega)^2 \left[ sq^5 e^{-is\phi_q} \right] + 2(i\omega)^2 \left( \gamma_{01}^2 - (i\omega)^2 \right) \left[ sq^3 e^{-is\phi_q} \right] + (i\omega)^2 \left( \gamma_{01}^2 - (i\omega)^2 \right)^2 \left[ sqe^{-is\phi_q} \right]. \tag{A8}$$

#### APPENDIX B: INTEGRALS TO DEFINE GREEN'S FUNCTIONS IN REAL SPACE

## 1. Integrals for the zeroth order

We can write the zeroth-order Green's function in real space as follows:

$$G_{0}(i\omega,r) = \begin{cases} i\omega((i\omega)^{2} - \gamma_{01}^{2})I_{00} - i\omega I_{03} & (i\omega)^{2}I_{01}^{-} - I_{04}^{-} & \gamma_{01}i\omega I_{00}^{-} & \gamma_{01}i\omega I_{00}^{-} \\ (i\omega)^{2}I_{01}^{+} - I_{04}^{+} & i\omega^{2}I_{00} - i\omega I_{03} & \gamma_{01}(i\omega)^{2}I_{00} & \gamma_{01}i\omega I_{01}^{-} \\ \gamma_{01}i\omega I_{01}^{+} & \gamma_{01}(i\omega)^{2}I_{00} & i\omega^{3}I_{00} - i\omega I_{03} & (i\omega)^{2}I_{01}^{-} - I_{04}^{-} \\ \gamma_{01}I_{02}^{+} & \gamma_{01}i\omega I_{01}^{+} & \gamma_{01}i\omega I_{01}^{+} & (i\omega)^{2}I_{01}^{+} - I_{04}^{+} & i\omega((i\omega)^{2} - \gamma_{01}^{-})I_{00} - i\omega I_{03} \\ \end{pmatrix}, \quad (B1)$$

$$I_{00} = \int_{0}^{+\infty} \frac{qdq}{2\pi} \int_{0}^{2\pi} \frac{d\phi_{q}}{q^{2}} \frac{e^{iq^{2}\cos(\phi_{q}-\phi_{p})}}{q^{2}-q^{2}(q^{2} - (i\omega)^{2} + \gamma_{01}i\omega)(q^{2} - (i\omega)^{2} - \gamma_{01}i\omega)}$$

$$= \int_{0}^{+\infty} \frac{dq}{2\pi} \int_{0}^{2\pi} \frac{q\phi_{q}}{q^{2}} \frac{qI_{0}(qr)}{q^{2}-q^{2}(e^{2})^{2} + \gamma_{01}i\omega)(q^{2} - (i\omega)^{2} - \gamma_{01}i\omega)}$$

$$= -\frac{1}{4\pi\gamma_{01}i\omega} [K_{0}(\Omega_{+}r) - K_{0}(\Omega_{-}r)], \quad (B2)$$

$$I_{01}^{\pm} = \int_{0}^{+\infty} \frac{qdq}{2\pi} \int_{0}^{2\pi} \frac{d\phi_{q}}{2\pi} \frac{sqe^{\pm is\phi_{q}}e^{iqr\cos(\phi_{q}-\phi_{p})}}{q^{2}-q^{2}(e^{2})^{2}-\gamma_{01}i\omega)(q^{2} - (i\omega)^{2} - \gamma_{01}i\omega)}$$

$$= \int_{0}^{+\infty} \frac{qdq}{2\pi} \frac{1}{(q^{2} - (i\omega)^{2} + \gamma_{01}i\omega)(q^{2} - (i\omega)^{2} - \gamma_{01}i\omega)}$$

$$= -\frac{ise^{\pm is\phi_{q}}}{4\pi\gamma_{01}i\omega} [\Omega_{+}^{2}K_{1}(\Omega_{+}r) - \Omega_{-}K_{1}(\Omega_{-}r)], \quad (B3)$$

$$I_{02}^{\pm} = \int_{0}^{+\infty} \frac{qdq}{2\pi} \frac{2^{2}}{q^{2}} \frac{d\phi_{q}}{(q^{2} - (i\omega)^{2} + \gamma_{01}i\omega)(q^{2} - (i\omega)^{2} - \gamma_{01}i\omega)}$$

$$= \int_{0}^{+\infty} \frac{qdq}{2\pi} \frac{2^{2\pi}}{(q^{2} - (i\omega)^{2} + \gamma_{01}i\omega)(q^{2} - (i\omega)^{2} - \gamma_{01}i\omega)}$$

$$= \int_{0}^{+\infty} \frac{qdq}{2\pi} \frac{2^{2\pi}}{(q^{2} - (i\omega)^{2} + \gamma_{01}i\omega)(q^{2} - (i\omega)^{2} - \gamma_{01}i\omega)}$$

$$= \int_{0}^{+\infty} \frac{qdq}{2\pi} \frac{2^{2\pi}}{(q^{2} - (i\omega)^{2} + \gamma_{01}i\omega)(q^{2} - (i\omega)^{2} - \gamma_{01}i\omega)}$$

$$= \int_{0}^{+\infty} \frac{qdq}{2\pi} \frac{2^{2\pi}}{(q^{2} - (i\omega)^{2} + \gamma_{01}i\omega)(q^{2} - (i\omega)^{2} - \gamma_{01}i\omega)}$$

$$= \int_{0}^{+\infty} \frac{qdq}{2\pi} \frac{2^{2\pi}}{(q^{2} - (i\omega)^{2} + \gamma_{01}i\omega)(q^{2} - (i\omega)^{2} - \gamma_{01}i\omega)}$$

$$= \int_{0}^{+\infty} \frac{qdq}{2\pi} \int_{0}^{2\pi} \frac{sq^{2}}{2\pi} \frac{sq^{2}e^{iqr\cos(\phi_{q}-\phi_{0})}}{(q^{2} - (i\omega)^{2} + \gamma_{01}i\omega)(q^{2} - (i\omega)^{2} - \gamma_{01}i\omega)}$$

$$= \int_{0}^{+\infty} \frac{dq}{2\pi} \int_{0}^{2\pi} \frac{sq^{2}}{2\pi} \frac{sq^{2}e^{iqr\cos(\phi_{q}-\phi_{0})}}{(q^{2} - (i\omega)$$

where we denoted  $\Omega_{\pm} = \sqrt{i\omega(\pm\gamma_{01} - i\omega)}$ , and  $K_i(z)$  is the *i*th modified Bessel function of the second kind.

## 2. Integrals for the first order

We can write componentwise the first-order Green's function in real space as follows:

$$G_1^{11} = \gamma_{03} \left[ -\gamma_{01} i\omega (I_{53}^+ + I_{53}^-) - \gamma_{01} i\omega \left( \gamma_{01}^2 - (i\omega)^2 \right) (I_{33}^+ + I_{33}^-) \right], \tag{B7}$$

$$G_1^{22} = \gamma_{03} \left[ -\gamma_{01} i\omega (I_{53}^+ + I_{53}^-) + \gamma_{01} (i\omega)^3 (I_{33}^+ + I_{33}^-) \right], \tag{B8}$$

$$G_1^{21} = \gamma_{03} \left[ -\gamma_{01} I_{64}^+ + \gamma_{01} (i\omega)^2 (I_{44}^+ - I_{42}^-) - \gamma_{01} (i\omega)^2 (\gamma_{01}^2 - (i\omega)^2) I_{22}^- \right], \tag{B9}$$

$$G_1^{31} = \gamma_{03} \left[ i\omega I_{62}^- + \gamma_{01}^2 i\omega I_{44}^+ + i\omega \left( \gamma_{01}^2 - 2(i\omega)^2 \right) I_{42}^- - (i\omega)^3 \left( \gamma_{01}^2 - (i\omega)^2 \right) I_{22}^- \right], \tag{B10}$$

$$G_1^{32} = \gamma_{03} \left[ I_{73}^{-} - 2(i\omega)^2 I_{53}^{-} + (i\omega)^4 I_{33}^{-} + \gamma_{01}^2 (i\omega)^2 I_{33}^{+} \right], \tag{B11}$$

$$G_1^{41} = \gamma_{03} \left[ \gamma_{01}^2 I_{55}^+ + (i\omega)^2 I_{51}^- + 2(i\omega)^2 (\gamma_{01}^2 - (i\omega)^2) I_{31}^- + (i\omega)^2 (\gamma_{01}^2 - (i\omega)^2)^2 I_{11}^- \right], \tag{B12}$$

$$G_1^{33} = G_1^{22}, \quad G_1^{44} = G_1^{11}, \quad G_1^{42} = G_1^{31}, \quad G_1^{43} = G_1^{21},$$
 (B13)

$$G_1^{12} = G_1^{34} = G_1^{21}(+ \leftrightarrow -), \quad G_1^{13} = G_1^{24} = G_1^{31}(+ \leftrightarrow -), \quad G_1^{14} = G_1^{41}(+ \leftrightarrow -), \quad G_1^{23} = G_1^{32}(+ \leftrightarrow -).$$
 (B14)

$$I_{11}^{\pm} = \int_{0}^{+\infty} \frac{qdq}{2\pi} \int_{0}^{2\pi} \frac{d\phi_{q}}{2\pi} \frac{sqe^{\pm is\phi_{q}}e^{iqr\cos(\phi_{q} - \phi_{r})}}{(q^{2} - (i\omega)^{2} + \gamma_{01}i\omega)^{2}(q^{2} - (i\omega)^{2} - \gamma_{01}i\omega)^{2}}$$

$$= \int_{0}^{+\infty} \frac{dq}{2\pi} \frac{ise^{\pm is\phi_{r}}q^{2}J_{1}(qr)}{(q^{2} - (i\omega)^{2} + \gamma_{01}i\omega)^{2}(q^{2} - (i\omega)^{2} - \gamma_{01}i\omega)^{2}}$$

$$= \frac{ise^{\pm is\phi_{r}}}{16\pi\gamma_{0}^{2}(i\omega)^{3}} [2(\Omega_{+}K_{1}(\Omega_{+}r) - \Omega_{-}K_{1}(\Omega_{-}r)) + i\omega\gamma_{01}r(K_{0}(\Omega_{+}r) + K_{0}(\Omega_{-}r))], \tag{B15}$$

$$\begin{split} I_{31}^{\pm} &= \int_{0}^{+\infty} \frac{q dq}{2\pi} \int_{0}^{2\pi} \frac{d\phi_{q}}{2\pi} \frac{sq^{3} e^{\pm is\phi_{q}} e^{iqr\cos(\phi_{q} - \phi_{r})}}{(q^{2} - (i\omega)^{2} + \gamma_{01}i\omega)^{2} (q^{2} - (i\omega)^{2} - \gamma_{01}i\omega)^{2}} \\ &= \int_{0}^{+\infty} \frac{dq}{2\pi} \frac{ise^{\pm is\phi_{r}} q^{4} J_{1}(qr)}{(q^{2} - (i\omega)^{2} + \gamma_{01}i\omega)^{2} (q^{2} - (i\omega)^{2} - \gamma_{01}i\omega)^{2}} \\ &= \frac{ise^{\pm is\phi_{r}}}{16\pi \gamma_{01}^{3} (i\omega)^{2}} \Big[ 2i\omega(\Omega_{+}K_{1}(\Omega_{+}r) - \Omega_{-}K_{1}(\Omega_{-}r)) - \gamma_{01}r(\Omega_{+}^{2}K_{0}(\Omega_{+}r) + \Omega_{-}^{2}K_{0}(\Omega_{-}r)) \Big], \end{split} \tag{B16}$$

$$\begin{split} I_{51}^{\pm} &= \int_{0}^{+\infty} \frac{q dq}{2\pi} \int_{0}^{2\pi} \frac{d\phi_{q}}{2\pi} \frac{sq^{5} e^{\pm is\phi_{q}} e^{iqr\cos(\phi_{q} - \phi_{r})}}{(q^{2} - (i\omega)^{2} + \gamma_{01}i\omega)^{2} (q^{2} - (i\omega)^{2} - \gamma_{01}i\omega)^{2}} \\ &= \int_{0}^{+\infty} \frac{dq}{2\pi} \frac{ise^{\pm is\phi_{r}} q^{6} J_{1}(qr)}{(q^{2} - (i\omega)^{2} + \gamma_{01}i\omega)^{2} (q^{2} - (i\omega)^{2} - \gamma_{01}i\omega)^{2}} \\ &= \frac{ise^{\pm is\phi_{r}}}{16\pi \gamma_{01}^{3} (i\omega)^{2}} \Big[ 2i\omega (\gamma_{01}^{2} - (i\omega)^{2}) (\Omega_{-}K_{1}(\Omega_{-}r) - \Omega_{+}K_{1}(\Omega_{+}r)) + \gamma_{01}r(\Omega_{+}^{4}K_{0}(\Omega_{+}r) + \Omega_{-}^{4}K_{0}(\Omega_{-}r)) \Big], \end{split} \tag{B17}$$

$$\begin{split} I_{22}^{\pm} &= \int_{0}^{+\infty} \frac{q dq}{2\pi} \int_{0}^{2\pi} \frac{d\phi_{q}}{2\pi} \frac{q^{2} e^{\pm 2is\phi_{q}} e^{iqr\cos(\phi_{q} - \phi_{r})}}{(q^{2} - (i\omega)^{2} + \gamma_{01}i\omega)^{2} (q^{2} - (i\omega)^{2} - \gamma_{01}i\omega)^{2}} \\ &= \int_{0}^{+\infty} \frac{dq}{2\pi} \frac{-e^{\pm 2is\phi_{r}} q^{3} J_{2}(qr)}{(q^{2} - (i\omega)^{2} + \gamma_{01}i\omega)^{2} (q^{2} - (i\omega)^{2} - \gamma_{01}i\omega)^{2}} \\ &= -\frac{e^{\pm 2is\phi_{r}}}{16\pi \gamma_{01}^{2} (i\omega)^{3}} \Big[ 2(\Omega_{+}^{2} K_{2}(\Omega_{+}r) - \Omega_{-}^{2} K_{2}(\Omega_{-}r)) + i\omega \gamma_{01} r(\Omega_{+} K_{1}(\Omega_{+}r) + \Omega_{-} K_{1}(\Omega_{-}r)) \Big], \end{split} \tag{B18}$$

$$\begin{split} I_{42}^{\pm} &= \int_{0}^{+\infty} \frac{q dq}{2\pi} \int_{0}^{2\pi} \frac{d\phi_{q}}{2\pi} \frac{q^{4} e^{\pm 2is\phi_{q}} e^{iqr\cos(\phi_{q} - \phi_{r})}}{(q^{2} - (i\omega)^{2} + \gamma_{01}i\omega)^{2} (q^{2} - (i\omega)^{2} - \gamma_{01}i\omega)^{2}} \\ &= \int_{0}^{+\infty} \frac{dq}{2\pi} \frac{-e^{\pm 2is\phi_{r}} q^{5} J_{2}(qr)}{(q^{2} - (i\omega)^{2} + \gamma_{01}i\omega)^{2} (q^{2} - (i\omega)^{2} - \gamma_{01}i\omega)^{2}} \\ &= -\frac{e^{\pm 2is\phi_{r}}}{16\pi \gamma_{01}^{3} (i\omega)^{2}} \Big[ 2i\omega (\Omega_{+}^{2} K_{2}(\Omega_{+}r) - \Omega_{-}^{2} K_{2}(\Omega_{-}r)) - \gamma_{01} r (\Omega_{+}^{3} K_{1}(\Omega_{+}r) + \Omega_{-}^{3} K_{1}(\Omega_{-}r)) \Big], \end{split} \tag{B19}$$

$$\begin{split} I_{cb}^{\pm} &= \int_{0}^{+\infty} \frac{gdq}{2\pi} \int_{0}^{2\pi} \frac{d\phi_q}{2\pi} \frac{q^5 e^{\frac{1}{2} \log_q} e^{\frac{1}{2} r \cos(\phi_q - \phi_b)}}{(q^2 - (i\omega)^2 + y_{01} i\omega)^2 (q^2 - (i\omega)^2 - y_{01} i\omega)^2} \\ &= \int_{0}^{+\infty} \frac{dq}{2\pi} \frac{-e^{\frac{1}{2} \log_q} q^2 + (i\omega)^2}{(2\pi (i\omega)^2 + y_{01} i\omega)^2 (2^2 - (i\omega)^2 - y_{01} i\omega)^2} \\ &= \frac{e^{\frac{1}{2} \log_q}}{15\pi \gamma_0^2 (i\omega)^2} \Big[ 2i\omega (y_0^2 - (i\omega)^2 + y_{01} i\omega)^2 (q^2 - (i\omega)^2 - y_{01} i\omega)^2 \\ &= \frac{e^{\frac{1}{2} \log_q}}{15\pi \gamma_0^2 (i\omega)^2} \Big[ 2i\omega (y_0^2 - (i\omega)^2 + y_{01} i\omega)^2 (q^2 - (i\omega)^2 - y_{01} i\omega)^2 \\ &= \int_{0}^{+\infty} \frac{gdq}{2\pi} \int_{0}^{2\pi} \frac{d\phi_q}{2\pi} \frac{sq^3 + ^{1+\log_q} e^{iq r \cos(\phi_q - \phi_q)}}{(q^2 - (i\omega)^2 + y_{01} i\omega)^2 (q^2 - (i\omega)^2 - y_{01} i\omega)^2} \\ &= \int_{0}^{+\infty} \frac{eq}{2\pi} \frac{q}{(q^2 - (i\omega)^2 + y_{01} i\omega)^2 (q^2 - (i\omega)^2 - y_{01} i\omega)^2} \\ &= \frac{ise^{\frac{1+\log_q}{2}}}{15\pi \gamma_0^2 (i\omega)^2} \Big[ 2i\omega_0^2 + X_0^2 (\omega)^2 + Y_0^2 (\omega)^2$$

#### APPENDIX C: T-MATRIX CALCULATION

With the help of  $G_0(i\omega, r)$  and  $G_1(i\omega, r)$  we can calculate the T matrix, whose expression is given by

$$T(i\omega) = \left[\mathbb{I} - V \cdot \lim_{r \to 0} G(i\omega, r)\right]^{-1} V. \tag{C1}$$

Here,  $G(i\omega, \mathbf{r}) = G_0(i\omega, \mathbf{r}) + G_1(i\omega, \mathbf{r})$ , and V takes one of the following forms:

with U denoting the magnitude of the impurity potential. At r = 0 the value of all the integrals that have angular dependence goes to zero; therefore  $G_1(i\omega, r = 0) = 0$ . Thus in order to determine the value of the T matrix, we need to calculate the following:

$$\lim_{r\to 0} G_0(i\omega, \mathbf{r}) = \lim_{r\to 0} \begin{pmatrix} i\omega \Big( (i\omega)^2 - \gamma_{01}^2 \Big) I_{00} - i\omega I_{03} & 0 & 0 & 0 \\ 0 & (i\omega)^3 I_{00} - i\omega I_{03} & \gamma_{01} (i\omega)^2 I_{00} & 0 \\ 0 & \gamma_{01} (i\omega)^2 I_{00} & (i\omega)^3 I_{00} - i\omega I_{03} & 0 \\ 0 & 0 & 0 & i\omega \Big( (i\omega)^2 - \gamma_{01}^2 \Big) I_{00} - i\omega I_{03} \end{pmatrix}. \quad (C2)$$

The limit above depends on  $\lim_{r\to+0} I_{00}$  and  $\lim_{r\to+0} I_{03}$ . For the first limit we get

$$\lim_{r \to +0} I_{00} = -\frac{1}{4\pi \gamma_{01} i\omega} \lim_{r \to +0} \left[ K_0(\Omega_+ r) - K_0(\Omega_- r) \right] = \frac{1}{4\pi \gamma_{01} i\omega} (\Omega_+ - \Omega_-). \tag{C3}$$

The second limit is given by

$$\lim_{r \to +0} I_{03} = \frac{1}{4\pi \gamma_{01} i\omega} \lim_{r \to +0} \left[ \Omega_{+}^{2} K_{0}(\Omega_{+}r) - \Omega_{-}^{2} K_{0}(\Omega_{-}r) \right] = \frac{1}{4\pi \gamma_{01} i\omega} \lim_{r \to +0} \left[ \Omega_{+}^{2} \left( -\gamma_{\mathcal{E}} - \ln \frac{\Omega_{+}r}{2} \right) - \Omega_{-}^{2} \left( -\gamma_{\mathcal{E}} - \ln \frac{\Omega_{-}r}{2} \right) \right] \\
= -\frac{1}{4\pi \gamma_{01} i\omega} \lim_{r \to +0} \left[ \gamma_{\mathcal{E}} \left( \Omega_{+}^{2} - \Omega_{-}^{2} \right) + \Omega_{+}^{2} \ln \frac{\Omega_{+}r}{2} - \Omega_{-}^{2} \ln \frac{\Omega_{-}r}{2} \right], \tag{C4}$$

where  $\gamma_{\mathcal{E}}$  is the Euler-Mascheroni constant. The expressions above display a logarithmic divergence at r=0, and we need to introduce a small-r cutoff. This divergence is a consequence of using a low-energy theory and losing the natural high-energy (small-distance) cutoff of the tight-binding model. The natural cutoff is  $r_c=a$ , where a is the lattice constant. Since we set the lattice constant to unity above, and all the distances are measured in those units, we can set  $r_c=1$ .

Finally, the resulting forms for the T matrices are given by

where we defined

$$f(i\omega) \equiv \frac{U}{1 - U \lim_{r \to +0} \left[ i\omega \left( (i\omega)^2 - \gamma_{01}^2 \right) I_{00} - i\omega I_{03} \right]}, \quad g(i\omega) \equiv \frac{U}{1 - U \lim_{r \to +0} \left[ (i\omega)^3 I_{00} - i\omega I_{03} \right]}.$$
 (C6)

## APPENDIX D: LOCAL DENSITY OF STATES

## 1. Real space

Asymptotically, at large r we have

$$\begin{split} \delta\rho_{A1}(\epsilon,r,\phi_r) &= -\frac{1}{\pi} \mathrm{Im} \bigg\{ \frac{f(i\omega)}{32\pi \ i\omega} \bigg[ \gamma_{01} \Big( \Omega_+ e^{-2\Omega_+ r} - \Omega_- e^{-2\Omega_- r} \Big) - 2i\omega \Big( \gamma_{01}^2 - i\omega \Big( i\omega - i\sqrt{\gamma_{01}^2 - (i\omega)^2} \Big) \Big) \frac{e^{-(\Omega_+ + \Omega_-) r}}{\sqrt{\Omega_-}\sqrt{\Omega_+}} \bigg] \frac{1}{r} \\ &+ \gamma_{03} \frac{f(i\omega)}{32\pi \ i\omega} \bigg[ \Omega_+^2 e^{-2\Omega_+ r} - \Omega_-^2 e^{-2\Omega_- r} + \sqrt{\Omega_+}\sqrt{\Omega_-}(\Omega_+ - \Omega_-) e^{-(\Omega_+ + \Omega_-) r} \Big] \frac{\sin 3\phi_r}{r} \bigg\}, \end{split} \tag{D1}$$

$$\begin{split} \delta\rho_{B1}(\epsilon,r,\phi_r) &= -\frac{1}{\pi} \text{Im} \left\{ \frac{g(i\omega)}{32\pi} \left[ i\omega \gamma_{01} \left( \frac{e^{-2\Omega_+ r}}{\Omega_+} - \frac{e^{-2\Omega_- r}}{\Omega_-} \right) + 2((i\omega)^2 + \Omega_+ \Omega_-) \frac{e^{-(\Omega_+ + \Omega_-) r}}{\sqrt{\Omega_+} \sqrt{\Omega_-}} \right] \frac{1}{r} \right. \end{aligned} \tag{D2} \\ &- \gamma_{03} \frac{g(i\omega)}{32\pi} \left[ (\gamma_{01} - i\omega)e^{-2\Omega_+ r} + (\gamma_{01} + i\omega)e^{-2\Omega_- r} + ((\gamma_{01} + i\omega)\Omega_+ + (\gamma_{01} - i\omega)\Omega_-) \frac{e^{-(\Omega_+ + \Omega_-) r}}{\sqrt{\Omega_+} \sqrt{\Omega_-}} \right] \frac{\sin 3\phi_r}{r} \right\}, \\ \delta\rho_{A2}(\epsilon, r, \phi_r) &= -\frac{1}{\pi} \text{Im} \left\{ \frac{g(i\omega)}{32\pi} \left[ i\omega \gamma_{01} \left( \frac{e^{-2\Omega_+ r}}{\Omega_+} - \frac{e^{-2\Omega_- r}}{\Omega_-} \right) - 2((i\omega)^2 + \Omega_+ \Omega_-) \frac{e^{-(\Omega_+ + \Omega_-) r}}{\sqrt{\Omega_+} \sqrt{\Omega_-}} \right] \frac{1}{r} \right. \\ &+ \gamma_{03} \frac{g(i\omega)}{32\pi \gamma_{01}^2} \left[ \left( \gamma_{01}^3 - 2i\omega \gamma_{01}^2 + 2(i\omega)^2 \gamma_{01} - (i\omega)^3 \right) e^{-2\Omega_+ r} + \left( \gamma_{01}^3 + 2i\omega \gamma_{01}^2 + 2(i\omega)^2 \gamma_{01} + (i\omega)^3 \right) e^{-2\Omega_- r} \right. \\ &- \left. \left( \left( \gamma_{01}^3 + 4i\omega \gamma_{01}^2 + 2(i\omega)^2 \gamma_{01} - (i\omega)^3 \right) \Omega_+ + \left( \gamma_{01}^3 - 4i\omega \gamma_{01}^2 + 2(i\omega)^2 \gamma_{01} + (i\omega)^3 \right) \Omega_- \right) \frac{e^{-(\Omega_+ + \Omega_-) r}}{\sqrt{\Omega_+} \sqrt{\Omega_-}} \right] \frac{\sin 3\phi_r}{r} \\ &+ \gamma_{03} \frac{g(i\omega)}{8\pi \gamma_{01}^3} i\omega \left( \gamma_{01}^2 - (i\omega)^2 \right) \left[ \frac{\gamma_{01} - i\omega}{\Omega_+} e^{-2\Omega_+ r} - \frac{\gamma_{01} + i\omega}{\Omega_-} e^{-2\Omega_- r} + 2i\omega \frac{e^{-(\Omega_+ + \Omega_-) r}}{\sqrt{\Omega_+} \sqrt{\Omega_-}} \right] \frac{\sin 3\phi_r}{r^2} \right\}, \tag{D3} \\ \delta\rho_{B2}(\epsilon, r, \phi_r) &= -\frac{1}{\pi} \text{Im} \left\{ \frac{f(i\omega)}{32\pi} \left[ \gamma_{01} \left( \frac{\gamma_{01} - i\omega}{\Omega_+} e^{-2\Omega_+ r} + \frac{\gamma_{01} + i\omega}{\Omega_-} e^{-2\Omega_- r} \right) + 2\left( \gamma_{01}^2 - (i\omega)^2 - \Omega_+ \Omega_- \right) \frac{e^{-(\Omega_+ + \Omega_-) r}}{\sqrt{\Omega_+} \sqrt{\Omega_-}} \right] \frac{1}{r} \\ &- \gamma_{03} \frac{f(i\omega)}{32\pi} \left[ (\gamma_{01} - i\omega)e^{-2\Omega_+ r} + (\gamma_{01} + i\omega)e^{-2\Omega_- r} + 3((\gamma_{01} + i\omega)\Omega_+ + (\gamma_{01} - i\omega)\Omega_-) \frac{e^{-(\Omega_+ + \Omega_-) r}}{\sqrt{\Omega_+} \sqrt{\Omega_-}} \right] \frac{\sin 3\phi_r}{r} \right\}. \tag{D3}$$

## 2. Momentum space

Below, we assume that the energy  $\epsilon > 0$ , and hence the terms with  $\Omega_{-}$  in Eqs. (18)–(21) provide the dominant contribution to the asymptotic behavior of the local density of states. If we chose negative energies, i.e.,  $\epsilon < 0$ , then the terms with  $\Omega_{+}$  would dominate. To perform Fourier transforms, we will use the two following integrals:

$$\mathcal{F}_{0}(p,\Omega) \equiv \mathcal{F}\left[\frac{e^{-\Omega r}}{r}\right] = \int d\mathbf{r} \frac{e^{-\Omega r}}{r} e^{-i\mathbf{p}\cdot\mathbf{r}} = \int_{0}^{\infty} dr e^{-\Omega r} \int_{0}^{2\pi} d\phi_{r} e^{-ipr\cos(\phi_{r}-\phi_{p})}$$

$$= 2\pi \int_{0}^{\infty} dr J_{0}(pr) e^{-\Omega r} = \frac{2\pi}{\Omega} \frac{1}{\sqrt{1+p^{2}/\Omega^{2}}},$$

$$\mathcal{F}_{1}(p,\phi_{p},\Omega) \equiv \mathcal{F}\left[\frac{e^{-\Omega r}}{r}\sin 3\phi_{r}\right] = \int d\mathbf{r} \frac{e^{-\Omega r}}{r}\sin 3\phi_{r} e^{-i\mathbf{p}\cdot\mathbf{r}} = \int_{0}^{\infty} dr e^{-\Omega r} \int_{0}^{2\pi} d\phi_{r}\sin 3\phi_{r} e^{-ipr\cos(\phi_{r}-\phi_{p})}$$

$$= 2\pi i \sin 3\phi_{p} \int_{0}^{\infty} dr J_{3}(pr) e^{-\Omega r} = 2\pi i \sin 3\phi_{p} \frac{p^{2}(-3+\sqrt{1+p^{2}/\Omega^{2}}) + 4\Omega^{2}(-1+\sqrt{1+p^{2}/\Omega^{2}})}{p^{3}\sqrt{1+p^{2}/\Omega^{2}}},$$
(D6)

where  $(p, \phi_p)$  are the polar coordinates in momentum space. Thus the Fourier transforms read

$$\delta\rho_{A1} = \frac{1}{2\pi i} \frac{f(\epsilon)\Omega_{-}[\gamma_{01}\mathcal{F}_{0}(p,2\Omega_{-}) + \gamma_{03}\Omega_{-}\mathcal{F}_{1}(\boldsymbol{p},2\Omega_{-})] - f^{*}(\epsilon)\Omega_{-}^{*}[\gamma_{01}\mathcal{F}_{0}(p,2\Omega_{-}^{*}) + \gamma_{03}\Omega_{-}^{*}\mathcal{F}_{1}(\boldsymbol{p},2\Omega_{-}^{*})]}{32\pi\epsilon}, \quad (D7)$$

$$\delta\rho_{B1} = \frac{1}{2\pi i} \gamma_{01} \frac{\frac{g(\epsilon)}{\Omega_{-}} [\epsilon \mathcal{F}_{0}(p, 2\Omega_{-}) + \gamma_{03}\Omega_{-}\mathcal{F}_{1}(\boldsymbol{p}, 2\Omega_{-})] - \frac{g^{*}(\epsilon)}{\Omega_{-}^{*}} [\epsilon \mathcal{F}_{0}(p, 2\Omega_{-}^{*}) + \gamma_{03}\Omega_{-}^{*}\mathcal{F}_{1}(\boldsymbol{p}, 2\Omega_{-}^{*})]}{32\pi},$$
(D8)

$$\delta \rho_{A2} = \frac{1}{2\pi i} \gamma_{01} \frac{\frac{g(\epsilon)}{\Omega_{-}} [\epsilon \mathcal{F}_{0}(p, 2\Omega_{-}) - \gamma_{03}\Omega_{-}\mathcal{F}_{1}(\boldsymbol{p}, 2\Omega_{-})] - \frac{g^{*}(\epsilon)}{\Omega_{-}^{*}} [\epsilon \mathcal{F}_{0}(p, 2\Omega_{-}^{*}) - \gamma_{03}\Omega_{-}^{*}\mathcal{F}_{1}(\boldsymbol{p}, 2\Omega_{-}^{*})]}{32\pi}, \tag{D9}$$

$$\delta \rho_{B2} = -\frac{1}{2\pi i} \gamma_{01} \frac{\frac{f(\epsilon)}{\Omega_{-}} [\gamma_{01} \mathcal{F}_{0}(p, 2\Omega_{-}) - \gamma_{03} \Omega_{-} \mathcal{F}_{1}(\mathbf{p}, 2\Omega_{-})] - \frac{f^{*}(\epsilon)}{\Omega_{-}^{*}} [\gamma_{01} \mathcal{F}_{0}(p, 2\Omega_{-}^{*}) - \gamma_{03} \Omega_{-}^{*} \mathcal{F}_{1}(\mathbf{p}, 2\Omega_{-}^{*})]}{32\pi}.$$
 (D10)

From the equations above we find the positions of ringlike resonances in momentum space. Indeed, both functions  $\mathcal{F}_0(p, 2\Omega_-)$  and  $\mathcal{F}_1(p, \phi_p, 2\Omega_-)$  have resonances at

$$p_{\rm res} = -2i\Omega_{-} = 2\sqrt{\epsilon(\gamma_{01} + \epsilon)}.$$
 (D11)

If we chose negative energies, i.e.,  $\epsilon < 0$ , then the resonances would appear at  $p_{\text{res}} = -2i\Omega_+ = 2\sqrt{|\epsilon|(\gamma_{01} + |\epsilon|)}$ .

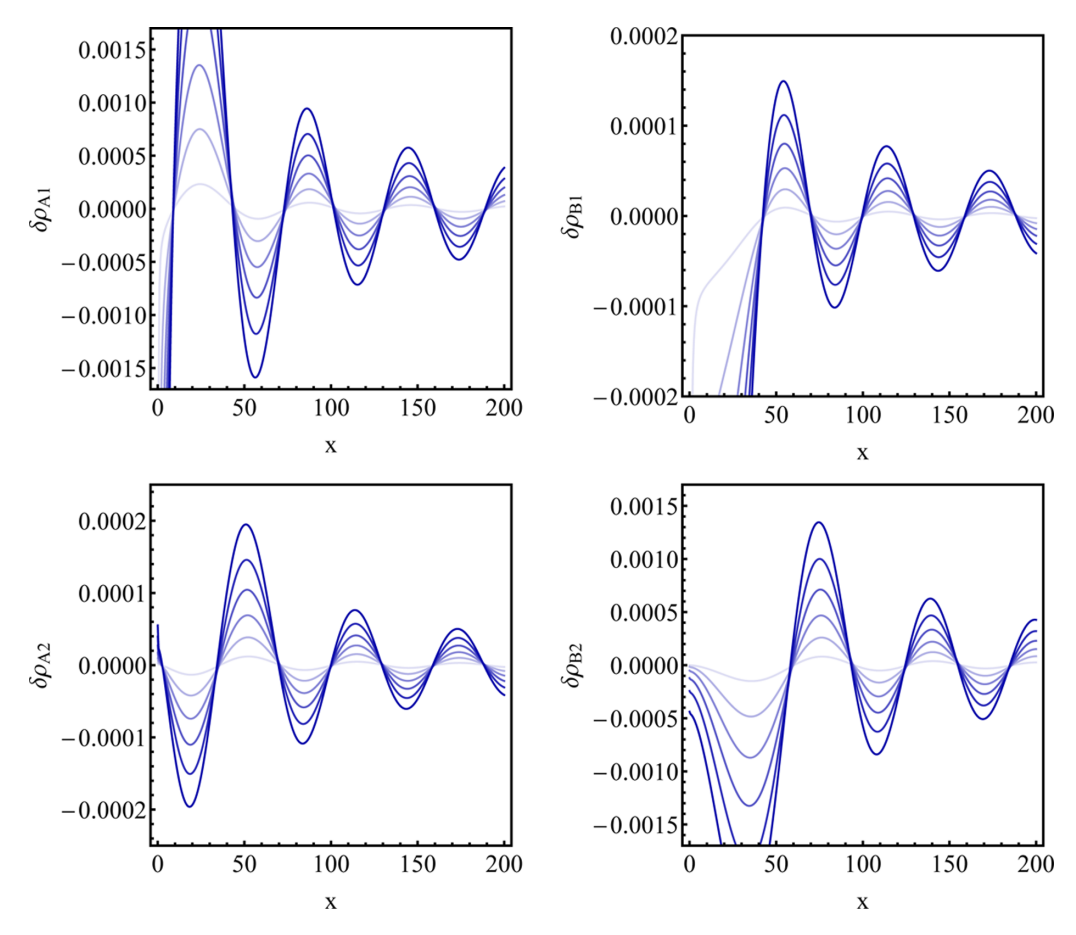


FIG. 5. Corrections to the local density of states calculated for A1, B1, A2, and B2 impurities, plotted as a function of x at y=0 taken in the units of interatomic distance  $a^*=a/\sqrt{3}=1.42$  Å. Curves of different shades correspond to different values of the impurity potential amplitude U, which varies from -3.5 to -38.5 in steps of 7. The larger is the absolute value of U, the darker is the corresponding curve. We set  $\gamma_{01}\approx0.15$ ,  $\gamma_{03}\approx-0.09$ ,  $\epsilon\approx0.018$ , which in dimensionful units corresponds to  $\gamma_1=0.42$  eV,  $\gamma_3=-3.3$  eV,  $\gamma_3=-3.3$  eV, and  $\gamma_1=0.42$  eV,  $\gamma_2=-3.3$  eV,  $\gamma_3=-3.3$  eV, and  $\gamma_1=0.42$  eV in steps of 20 eV.

# APPENDIX E: DEPENDENCE ON IMPURITY POTENTIAL AMPLITUDE $\boldsymbol{U}$

Here, we show that the results in Fig. 3 for the local density of states in the presence of different types of impurities depend only quantitatively and not qualitatively on the impurity potential amplitude U. In Fig. 5 we set y = 0, and we plot cuts of the plots in Fig. 3 along the x axis for different values of the impurity potential amplitude U. It is clear from the panels that the main difference between different values of U manifests in the amplitudes of the oscillatory patterns, while the periods remain the same in the asymptotic limit.

- [1] J. Friedel, Nuovo Cimento 7, 287 (1958).
- [2] V. V. Cheianov and V. I. Fal'ko, Phys. Rev. Lett. 97, 226801 (2006).
- [3] E. Mariani, L. I. Glazman, A. Kamenev, and F. von Oppen, Phys. Rev. B **76**, 165402 (2007).
- [4] S. A. Kivelson, I. P. Bindloss, E. Fradkin, V. Oganesyan, J. M. Tranquada, A. Kapitulnik, and C. Howald, Rev. Mod. Phys. 75, 1201 (2003).
- [5] C. Bena and S. A. Kivelson, Phys. Rev. B 72, 125432 (2005).
- [6] C. Bena, Phys. Rev. Lett. 100, 076601 (2008).
- [7] C. Bena, Phys. Rev. B **79**, 125427 (2009).
- [8] T. O. Wehling, A. V. Balatsky, M. I. Katsnelson, A. I. Lichtenstein, K. Scharnberg, and R. Wiesendanger, Phys. Rev. B 75, 125425 (2007).

- [9] N. M. R. Peres, F. Guinea, and A. H. Castro Neto, Phys. Rev. B 73, 125411 (2006).
- [10] N. M. R. Peres, F. D. Klironomos, S.-W. Tsai, J. R. Santos, J. M. B. L. dos Santos, and A. H. C. Neto, EPL (Europhys. Lett.) 80, 67007 (2007).
- [11] M. A. H. Vozmediano, M. P. López-Sancho, T. Stauber, and F. Guinea, Phys. Rev. B 72, 155121 (2005).
- [12] T. Ando, J. Phys. Soc. Jpn. 75, 074716 (2006).
- [13] Y. Pogorelov, arXiv:cond-mat/0603327.
- [14] Y. V. Skrypnyk and V. M. Loktev, Phys. Rev. B **73**, 241402(R)
- [15] Y. V. Skrypnyk and V. M. Loktev, Phys. Rev. B 75, 245401 (2007).

- [16] M. Katsnelson and A. Geim, Philos. Trans. R. Soc., A 366, 195 (2007).
- [17] C. Dutreix and M. I. Katsnelson, Phys. Rev. B 93, 035413 (2016).
- [18] P. Mallet, F. Varchon, C. Naud, L. Magaud, C. Berger, and J.-Y. Veuillen, Phys. Rev. B 76, 041403(R) (2007).
- [19] P. Mallet, I. Brihuega, V. Cherkez, J. M. Gómez-Rodríguez, and J.-Y. Veuillen, C. R. Phys. 17, 294 (2016).
- [20] J.-C. Charlier, X. Gonze, and J.-P. Michenaud, Phys. Rev. B 43, 4579 (1991).
- [21] E. McCann and V. I. Fal'ko, Phys. Rev. Lett. **96**, 086805 (2006).
- [22] E. McCann and M. Koshino, Rep. Prog. Phys. 76, 056503 (2013).
- [23] A. B. Kuzmenko, I. Crassee, D. van der Marel, P. Blake, and K. S. Novoselov, Phys. Rev. B 80, 165406 (2009).
- [24] F. Joucken, Z. Ge, E. A. Quezada-López, J. L. Davenport, K. Watanabe, T. Taniguchi, and J. Velasco, Phys. Rev. B 101, 161103(R) (2020).
- [25] A. A. Zibrov, P. Rao, C. Kometter, E. M. Spanton, J. I. A. Li, C. R. Dean, T. Taniguchi, K. Watanabe, M. Serbyn, and A. F. Young, Phys. Rev. Lett. 121, 167601 (2018).
- [26] A. Varlet, D. Bischoff, P. Simonet, K. Watanabe, T. Taniguchi, T. Ihn, K. Ensslin, M. Mucha-Kruczyński, and V. I. Fal'ko, Phys. Rev. Lett. 113, 116602 (2014).
- [27] M. Orlita, P. Neugebauer, C. Faugeras, A.-L. Barra, M. Potemski, F. M. D. Pellegrino, and D. M. Basko, Phys. Rev. Lett. 108, 017602 (2012).

- [28] Y. Shi, S. Che, K. Zhou, S. Ge, Z. Pi, T. Espiritu, T. Taniguchi, K. Watanabe, Y. Barlas, R. Lake, and C. N. Lau, Phys. Rev. Lett. 120, 096802 (2018).
- [29] K. Kechedzhi, V. I. Fal'ko, E. McCann, and B. L. Altshuler, Phys. Rev. Lett. 98, 176806 (2007).
- [30] Z. Ge, F. Joucken, E. Quezada, D. R. da Costa, J. Davenport, B. Giraldo, T. Taniguchi, K. Watanabe, N. P. Kobayashi, T. Low, and J. Velasco, Nano Lett. 20, 8682 (2020).
- [31] J. Jung and A. H. MacDonald, Phys. Rev. B 89, 035405 (2014).
- [32] J. M. Byers, M. E. Flatté, and D. J. Scalapino, Phys. Rev. Lett. 71, 3363 (1993).
- [33] M. I. Salkola, A. V. Balatsky, and D. J. Scalapino, Phys. Rev. Lett. 77, 1841 (1996).
- [34] W. Ziegler, D. Poilblanc, R. Preuss, W. Hanke, and D. J. Scalapino, Phys. Rev. B 53, 8704 (1996).
- [35] G. D. Mahan, Many-Particle Physics (Springer, New York, 2000).
- [36] A. V. Balatsky, I. Vekhter, and J.-X. Zhu, Rev. Mod. Phys. 78, 373 (2006).
- [37] C. Bena, C. R. Phys. 17, 302 (2016).
- [38] F. Joucken, C. Bena, Z. Ge, E. Quezada-Lopez, S. Pinon, V. Kaladzhyan, T. Taniguchi, K. Watanabe, A. Ferreira, and J. Velasco, Nano Lett. 21, 7100 (2021).
- [39] V. Kaladzhyan, S. Pinon, F. Joucken, Z. Ge, E. A. Quezada-Lopez, T. Taniguchi, K. Watanabe, J. Velasco, and C. Bena, Phys. Rev. B 104, 155418 (2021).